Stability of lattice Boltzmann methods in hydrodynamic regimes

Rodney A. Worthing, Joel Mozer, and Guy Seeley
Phillips Laboratory, Hanscom Air Force Base, Bedford, Massachusetts 01730
(Received 29 August 1996; revised manuscript received 13 May 1997)

The Von Neumann linear stability theory as applied by Sterling and Chen [J. Comput. Chem. **123**, 196 (1996)] to lattice Boltzmann numerical methods is revisited and extended. A simplifying assumption made by these authors (on the character of the most unstable mode) is abandoned and immediate refinements on their stability results are attained. The inadequacy of uniform background flow, as a general point of expansion, is evident from simulations of simple shear waves. The stability theory is consequently extended to address the destabilizing role of ''background'' shear. To this end, exact time-dependent solutions of the nine-velocity Bhatnagar-Gross-Krook (BGK) lattice Boltzmann model (LB9) are derived and used as expansion points for the stability theory. Calculations reveal both physical and nonphysical instabilities, the former being interpreted via classical inviscid stability theory and the latter forming an empirical *instability* criterion (fitting better at small values of the viscosity), $N<R^{0.56}$, where N is the number of mesh points in the shearing direction and R is the flow Reynolds number. This is interestingly close to the Kolmogorov-Batchelor-Kraichnan inertial range cutoff $R^{1/2}$ for two-dimensional isotropic turbulence. In this case, stability seems to require at least the spatial resolution required for accuracy. We also note that the particular class of solutions found above for the LB9 model can be compared directly to corresponding solutions of the Navier-Stokes equations. It is demonstrated that setting $\tau=1$, where τ is the relaxation time of the BGK collision operator, provides optimal accuracy in time. This observation may be relevant to current studies as letting $\tau\rightarrow 1/2$ appears to be a common technique aimed at lowering the viscosity and thereby increasing the Reynolds number of LB simulations. [S1063-651X(97)11608-7]

PACS number(s): 47.11.+j, 02.70.Ns

I. INTRODUCTION

This paper addresses the numerical stability of the lattice Boltzmann [2–5] class of simulation techniques designed to approximate, in its macrodynamics, the equations of fluid dynamics. The lattice Boltzmann (LB) method (which models the probability density of particles) and its predecessor, the lattice-gas (LG) method (which models an integer number of particles [6]), are arguably the simplest and most general computational techniques available for hydrodynamics. In the spirit of the kinetic theory of gases, both the LG and LB methods propose to simulate particle dynamics, but with movements confined to a specified spatial lattice. During a fundamental time step, usually set to unity, particles may advance only to a relatively predefined set of nearby nodes $\mathbf{x}+\mathbf{e}_d$ with $d=0,\ldots,d_{\max}$, and in this manner particle velocities are limited and discrete. At the end of the time step, conservative collisions are imagined to occur at each node whereby mass is redistributed amongst the velocity set in preparation for the next ''streaming'' step. It has been demonstrated [4] that such models can, at large scales, approximate the Navier-Stokes equations.

In this article focus will be on the more efficient LB method with *linearized* collision operator [3,5] since it has been observed that the scale at which Navier-Stokes-type behavior is recognized is greatly reduced here compared to that of the LG methods [7] and that the computational cost of the collision calculations is greatly reduced here compared to that of the strict LB formulation [2], making the scheme comparable in efficiency to conventional spectral methods [8]. Apparently the price paid for these marked improvements is the introduction of numerical instabilities. LB proponents have mainly reported on simulations in stable regimes or on cases where instabilities are ''flushed'' out of the system before maturing. Some authors [3,9] have even suggested, based on a stability analysis about zero flow, that such schemes are actually stable. Yet it is common, if not tacit, knowledge among LB practitioners that instabilities are present and impede the aggressive application of these methods to many hydrodynamic regimes.

This broaches an interesting point concerning the goals of a stability analysis. The task of delineating the exact region of parameter space that is stable, for all possible flow conditions, seems unattainable. That digested, declaring any region stable (without many qualifiers) seems misleading. Perhaps a more reasonable though certainly more modest approach is to delineate regions that are clearly *unstable*. As more and more initial fields are analyzed this region can be refined, but still it retains its basic property that somewhere, somehow, something has gone unstable within.

Both the streaming and collision steps of the LB method

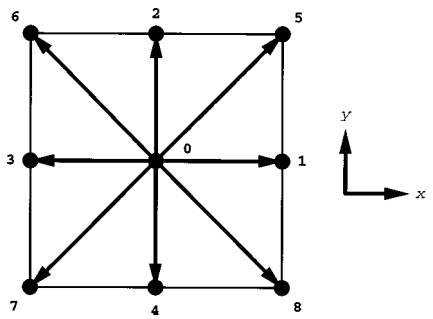

FIG. 1. The LB9 lattice configuration.

described above can be combined in the single formula

$$f_d(\mathbf{x}+\mathbf{e}_d,t+1)=f_d(\mathbf{x},t)+\Omega_{ds}\{f_s(\mathbf{x},t) - F_s(n(\mathbf{x},t),\mathbf{m}(\mathbf{x},t))\}, \quad (1)$$

where $f_d(\mathbf{x},t)$ is defined only at the nodes and represents the mass of particles currently moving from node $\mathbf{x}$ with the prescribed velocity $\mathbf{e}_d$. The presumed local equilibrium distribution $\mathbf{F}$ (which represents an attempt in extrapolation of thermodynamic equilibrium to the presence of a small imposed velocity $\mathbf{u}$) is a function of $\mathbf{f}$ only through local macroscopic quantities like mass $n=\Sigma_d f_d$ and momentum $\mathbf{m}=n\mathbf{u}=\Sigma_d f_d \mathbf{e}_d$. The role of the collision term $\mathbf{\Omega}[\mathbf{f}-\mathbf{F}]$ is to nudge the system towards local equilibrium $\mathbf{F}$ in a manner consistent with the local conservation principles of mass and momentum,

$$\sum_d f_d(\mathbf{x}+\mathbf{e}_d,t+1)=\sum_d f_d(\mathbf{x},t), \quad (2)$$

$$\sum_d \mathbf{e}_d f_d(\mathbf{x}+\mathbf{e}_d,t+1)=\sum_d \mathbf{e}_d f_d(\mathbf{x},t), \quad (3)$$

and energy in thermally cognizant models. As neither the collision operator $\mathbf{\Omega}$, the local equilibrium distribution function $\mathbf{F}$, nor the lattice structure is uniquely determined by requiring Navier-Stokes behavior at large scale, many different models have been and continue to be examined in the literature. It is hoped that the work presented here will help provide guidance, based on stability considerations, in the choice of an optimal model. Two popular two-dimensional (2D) models (see Appendix A), the seven-velocity triangular lattice model LB7 and the nine-velocity, square lattice model LB9 (see Fig. 1), also considered by in [1], are investigated in detail. Both of these models are said to have a single relaxation time or Bhatnagar-Gross-Krook (BGK) [10] type linearized collision operator of the simple form

$$\mathbf{\Omega}=-\frac{1}{\tau}\mathbf{I}, \quad (4)$$

where $\mathbf{I}$ in the identity operator and τ is the relaxation parameter. There are no conceptual difficulties extending the techniques presented here to higher dimensions and/or more general models.

II. LINEAR STABILITY THEORY

A natural starting place for a stability analysis is a rectangular periodic domain. Such domains are typically more amenable mathematically than others and often used in numerical and theoretical studies as an apology for the infinite domain. Periodicity of Fourier modes allows for a simplified stability theory in which the boundary conditions are satisfied automatically. The up side of this is that fundamental modes of the dynamical system may be investigated in isolation, without the added complication of boundary conditions. The down side is, of course, that boundary conditions clearly do alter the modes of a system (though sometimes not too dramatically) and these alterations as well as their role in initiating instabilities remain unaddressed.

Suppose the LB dynamics are confined to a regular lattice roughly filling a rectangular region of space defined by

$$0\leqslant x<L_x, \quad 0\leqslant y<L_y, \quad (5)$$

where the smallest node-node distance is conventionally taken to be 1. For purposes of the stability theory it is convenient to introduce another, perhaps finer, $N_x\times N_y$ *rectangular* mesh defined as the smallest which contains the nodes of the original dynamical lattice. The probability distribution function $f_d(x,y,t)$ of the lattice Boltzmann method is defined only at the appropriate subset of the nodal values

$$x=\left(0\times\frac{L_x}{N_x},1\times\frac{L_x}{N_x},\ldots,(N_x-1)\times\frac{L_x}{N_x}\right) \quad \text{cross}$$

$$y=\left(0\times\frac{L_y}{N_y},1\times\frac{L_y}{N_y},\ldots,(N_y-1)\times\frac{L_y}{N_y}\right). \quad (6)$$

The stability of the dynamical system

$$f_d(\mathbf{x}+\mathbf{e}_d,t+1)-f_d(\mathbf{x},t)=-\frac{1}{\tau}[f_d(\mathbf{x},t)-F_d(\mathbf{x},t)]+B_d(\mathbf{x},t) \quad (7)$$

is investigated near a completely arbitrary given distribution $f_d(\mathbf{x},t)=\mathcal{F}_d(\mathbf{x})$. In Eq. (7), F_d represents a local equilibrium distribution and B_d represents corrections due to body forces like gravity. For any specific model, both F_d and B_d are prescribed functions of $\mathbf{f}$, though this dependence is not explicitly shown.

Expanding near $\mathcal{F}_d(\mathbf{x})$ by writing

$$f_d(\mathbf{x},t)=\mathcal{F}_d(\mathbf{x})+f'_d(\mathbf{x},t), \quad (8)$$

one finds, to first order in $\mathbf{f}'$,

$$f'_d(\mathbf{x}+\mathbf{e}_d,t+1)=G_d(\mathbf{x})+\left(1-\frac{1}{\tau}\right)f'_d(\mathbf{x},t) + \sum_s J_{ds}(\mathbf{x})f'_s(\mathbf{x},t), \quad (9)$$

where

$$G_d(\mathbf{x})\equiv\mathcal{F}_d(\mathbf{x})-\mathcal{F}_d(\mathbf{x}+\mathbf{e}_d)+B_d|_{\mathcal{F}}+\frac{1}{\tau}[F_d|_{\mathcal{F}}-\mathcal{F}_d(\mathbf{x})] \quad (10)$$

and the combined Jacobian is

$$J_{ds}(\mathbf{x})\equiv\left[\frac{1}{\tau}\frac{\partial F_d}{\partial f_s}+\frac{\partial B_d}{\partial f_s}\right]_{\mathcal{F}}. \quad (11)$$

Except for special cases, like an initially uniform distribution, $G_d(\mathbf{x})$ will be nonzero; nevertheless, this inhomogeneous term apparently only contributes algebraic growth and can be safely ignored when characterizing the more rapid exponential type instabilities commonplace to the LB schemes. So doing results in the homogeneous, nonconstant coefficient difference equation

$$f_d'(\mathbf{x}+\mathbf{e}_d,t+1)=\left(1-\frac{1}{\tau}\right)f_d'(\mathbf{x},t)+\sum_s J_{ds}(\mathbf{x})f_s'(\mathbf{x},t). \tag{12}$$

A complete Fourier representation [11] of the state of the system (at the nodes) can be written

$$f_d'(x,y,t)=\sum_{k_x,k_y} f_d^{(k_x,k_y)}e^{ik_x(2\pi/L_x)x}e^{ik_y(2\pi/L_y)y}, \tag{13}$$

where wave numbers k_x and k_y loop over their allowable integer values:

$$-\frac{N_x}{2}\leqslant k_x\leqslant\frac{N_x}{2}-1, \quad -\frac{N_y}{2}\leqslant k_y\leqslant\frac{N_y}{2}-1. \tag{14}$$

In this paper, the case where $\mathcal{F}$, and so the initial mean quantities, depends only the single coordinate y is considered. Incorporating this simplification into Eq. (12) and expanding the resulting Jacobian in its own Fourier series,

$$J_{ds}(y)=\sum_{K_y}\mathcal{J}_{ds}^{(K_y)}e^{iK_y(2\pi/L_y)y}, \quad -\frac{N_y}{2}\leqslant K_y\leqslant\frac{N_y}{2}-1, \tag{15}$$

gives

$$e^{ik_x(2\pi/N_x)x_d}e^{ik_y(2\pi/N_y)y_d}f_d^{(k_x,k_y)}(t+1)$$

$$=\left(1-\frac{1}{\tau}\right)f_d^{(k_x,k_y)}(t)+\mathcal{J}_{ds}^{(K_y)}f_s^{(k_x,k_y-K_y)}(t), \tag{16}$$

where the components of velocity vectors have been denoted by $\mathbf{e}_d=x_d\mathbf{i}+y_d\mathbf{j}$.

Since the x modes remain uncoupled, they are considered independently via

$$e^{ik_x(2\pi/N_x)x_d}e^{ik_y(2\pi/N_y)y_d}f_d^{(k_y)}(t+1)$$

$$=\left(1-\frac{1}{\tau}\right)f_d^{(k_y)}(t)+\mathcal{J}_{ds}^{(K_y)}f_s^{(k_y-K_y)}(t). \tag{17}$$

In the Galerkin manner, the highest y harmonics arising from the convolution term are ignored [12] allowing Eq. (17) to be written as a matrix iteration

$$\mathbf{f}_{t+1}=\mathcal{A}\mathbf{f}_t, \tag{18}$$

where the vector $\mathbf{f}$ has components $f_d^{(k_y)}$. If the spectral radius of $\mathcal{A}$, $\rho(\mathcal{A})$, is larger than unity, then the system is said to be linearly unstable.

III. INSTABILITY ASSOCIATED WITH UNIFORM BACKGROUND FLOW

A. Nonlinear instability

It turns out that a very general (independent of the choice of $\mathbf{F}$) statement of instability in terms of the eigenspectrum of the collision operator $\mathbf{\Omega}$ in Eq. (1) can be made: If there exists an eigenvalue λ of $\mathbf{\Omega}$ such that $\lambda<-2$ or $\lambda>0$, then at least certain initial value problems (1) will be unstable. This point is demonstrated by analyzing the particular problem of a uniform initial condition. In one way or another, other authors [9,5,1] have come to an identical criterion; however, it is hoped that the discussion that follows helps to clarify this instability. The theory is completely nonlinear in that no assumption concerning the proximity of the particle density distribution to equilibrium is necessary.

Inspection of the evolution equation (1) shows that an initially uniform flow, in the sense that

$$f_d(\mathbf{x},t_0)=f_d(t_0), \tag{19}$$

will remain uniform at all later times. Furthermore, local conservation principles, Eqs. (2) and (3), then demand that both $n(\mathbf{x},t)$ and $\mathbf{m}(\mathbf{x},t)$, which are always conserved globally in a periodic domain, retain their initial constant values, $n(\mathbf{x},t)=n_0$ and $\mathbf{m}(\mathbf{x},t)=\mathbf{m}_0$. As F_d is only a function of these macroscopic quantities, it too remains fixed in space and time. For this class of initial conditions, it therefore follows that Eq. (1) is mathematically [13] equivalent to

$$f_d(t+1)=f_d(t)+\Omega_{ds}\{f_s(t)-F_s(n_0,\mathbf{m}_0)\} \tag{20}$$

and can be rewritten as

$$\tilde{\mathbf{f}}(t+1)=[\mathbf{I}+\mathbf{\Omega}]\tilde{\mathbf{f}}(t), \tag{21}$$

where the vector $\tilde{\mathbf{f}}$ has components $f_d(t)-F_d[n_0,\mathbf{m}_0]$. The iteration equation (21) reveals unbounded growth if the spectral radius of $[\mathbf{I}+\mathbf{\Omega}]$ exceeds unity, leading to the aforementioned criterion on the spectrum of $\mathbf{\Omega}$. For the BGK collision operator (4) the instability criterion becomes $\tau<1/2$ and can typically be interpreted as a negativity condition on the mac-

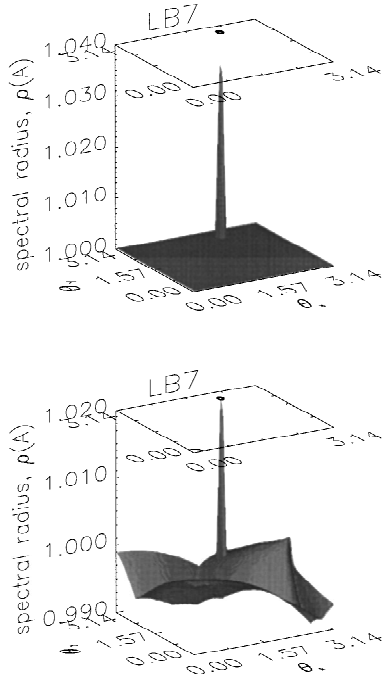

FIG. 2. Top: Growth rates for LB7 show that the most unstable wave number for $\tau=0.5$ at $\alpha=0.6$ and $U=0.2$ has both x and y dependence. Bottom: Similar to the top, but with $\tau=0.505$ intended to demonstrate the continuation of the $\rho(\mathcal{A})$ surface in the $\tau\rightarrow1/2$ limit.

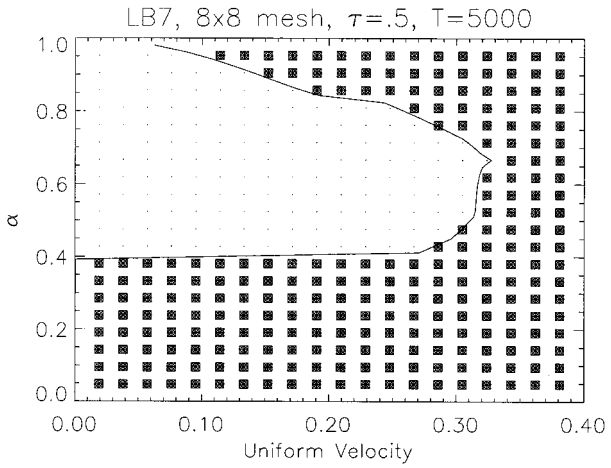

FIG. 3. LB7 stability boundary curve compared to time simulations on an 8×8 mesh. The squares designate initial conditions that have become clearly unstable by the time given in the figure.

roscopic kinematic viscosity (see Appendix A for specific formulas) making it analogous to the blowup of the notorious backwards diffusion equation $\partial_t f=-\nabla^2 f$. In contrast, typical numerical instabilities rely on the introduction of small amplitude noise (via round-off) and depend on the mean state of the system for energy. These types of instabilities are analyzed in the remainder of this section using linear stability theory.

B. Linear instability

The logic leading to Eq. (20) breaks down if the initial uniform distribution is contaminated with the tiniest amount of nonuniformity, opening the door to spatially dependent instabilities. Consider a uniform velocity field $\mathbf{u}=U\hat{\mathbf{i}}$ as the point of expansion. For nonthermal models, $\mathbf{F}$ is typically a function of both $\mathbf{u}$ and n while its Jacobian $\mathbf{J}$ depends only on $\mathbf{u}$ (see Appendix A). This allows for a generalization of the results that follow to arbitrary density profiles $n(x,y)$.

The y independence of the selected background velocity is carried over to the Jacobian [i.e., $K_y=0$ is the only surviving term in its expansion (15)], leading to decoupling of

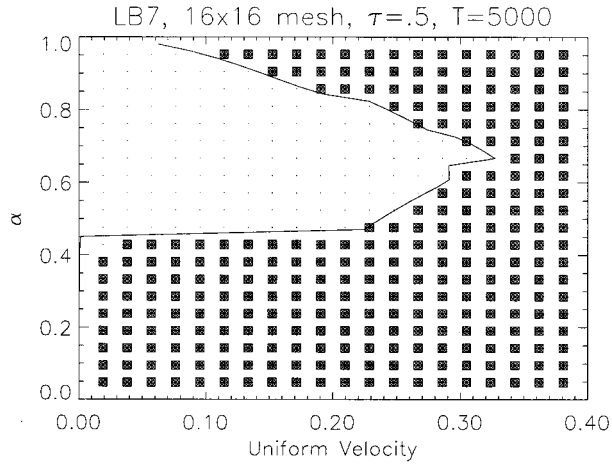

FIG. 4. Same as Fig. 3 but with a mesh size of 16×16.

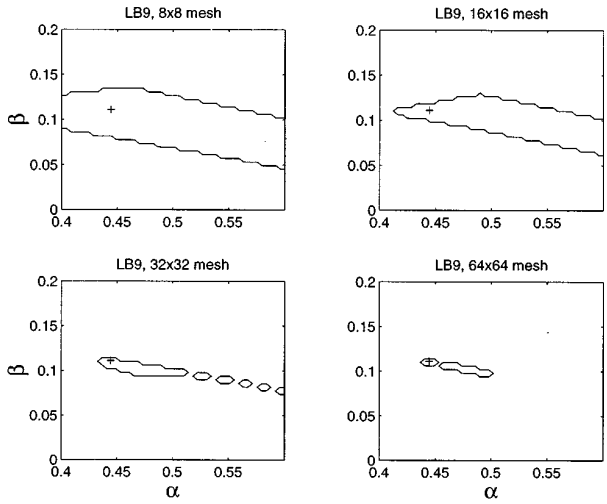

FIG. 5. Results for LB9, showing the stable (to uniform flow) values of the free parameters α and β. As the mesh size is increased the region of stability diminishes. The pair used by Martinez *et al.* [8] ($\alpha=\frac{4}{9}$, $\beta=\frac{1}{9}$) is marked with $+$.

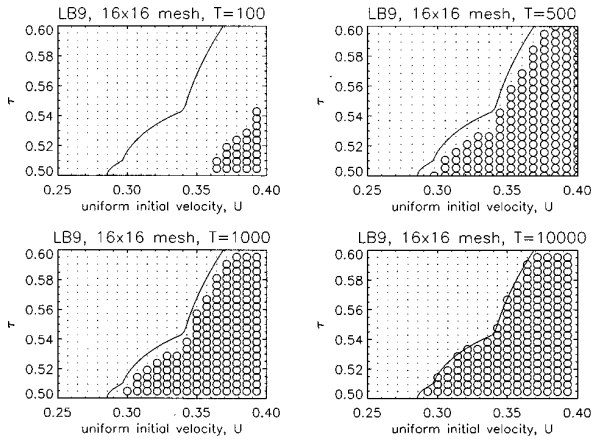

FIG. 6. LB9 neutral stability curve and simulations for $\tau=1/2$. A ''○'' designates an initial condition that is found to be unstable by the time T given in the title of each plot.

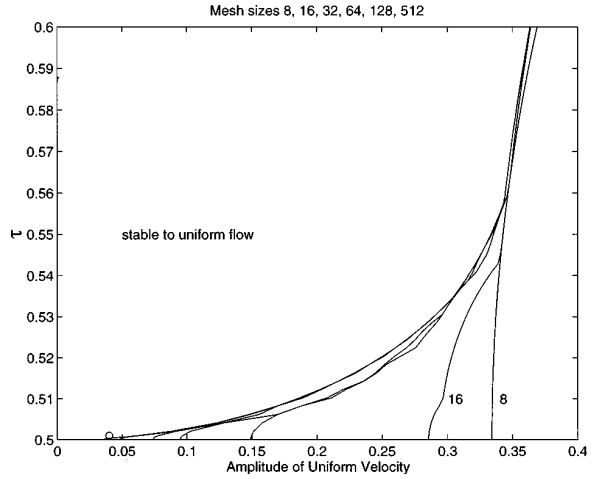

FIG. 7. LB9 stability boundary curves for uniform flow at various mesh sizes. The 2D ''turbulent'' simulation of Martinez *et al.* [8] on a 512×512 mesh is designated by a ''○'' and lies just stable of the corresponding neutral stability curve.

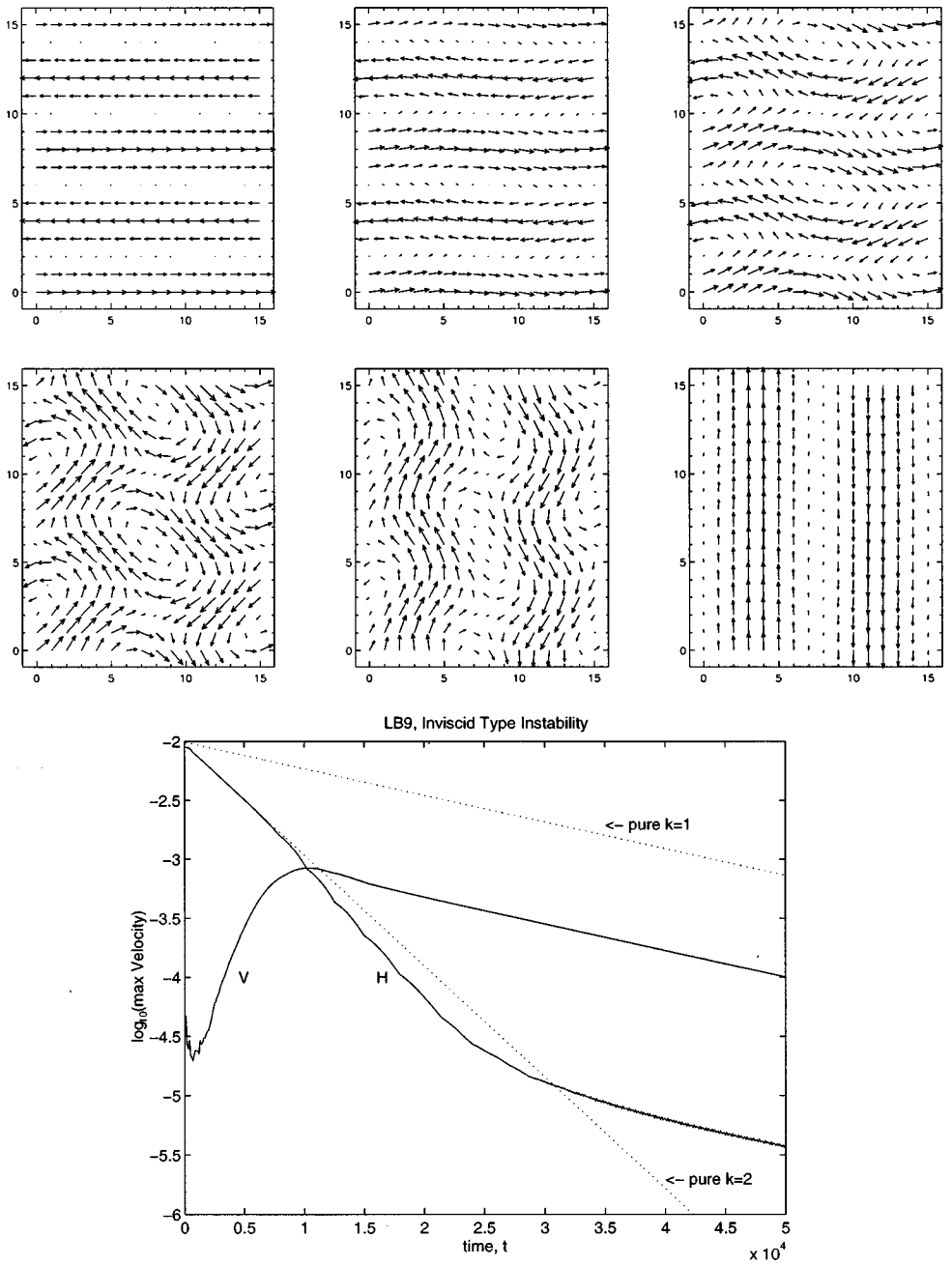

FIG. 8. Velocity vector diagrams displaying an inviscid-type instability. Time increases from left to right with the values $t=0$ and 6000, 8000, 10 000, 12 000, and 40 000. Maximal horizontal (H) and vertical (V) velocities for this simulation are plotted as solid curves. At $t=0$ the distribution was assigned the equilibrium distribution for a pure $k=2$ horizontal flow of amplitude 10^{-2} and then contaminated with 10^{-5} random noise. The dotted lines are similar simulations but with significantly smaller noise and intended to help clarify the above dynamics via rate-of-dissipation comparisons.

the y modes in Eq. (17). By considering these modes independently, as discussed previously for the x modes, the dimension of system (18) is reduced by a factor of N_y, and one arrives at the matrix investigated by Sterling and Chen [1],

$$\mathcal{A}=\mathbf{D}\left[\left(1-\frac{1}{\tau}\right)\mathbf{I}+\mathbf{J}\right], \tag{22}$$

where $\mathbf{D}$ is a diagonal matrix with entries

$$D_{ds}=e^{-i(\theta_x x_d+\theta_y y_d)}\delta_{d,s} \tag{23}$$

and $\theta_x\equiv 2\pi k_x/N_x$ and $\theta_y\equiv 2\pi k_y/N_y$ are ''relative'' wave numbers. Instability occurs if

$$\max_{\theta_x,\theta_y}\rho(\mathcal{A}[\theta_x,\theta_y,U,\tau,\alpha,\beta])>1. \tag{24}$$

The last two arguments in the list above represent free parameters that can ultimately be chosen, for example, to improve a model's stability characteristics. The maximization is over all *allowable* wave numbers (14), and it is only

through this restriction [14] that the size of the lattice continues to enter into the stability problem for uniform flow. As the mesh size increases, θ_x and θ_y approach continuous variables on $(-\pi,\pi]$. If the above maximization is considered over the continuous variables, then all possible meshes will have been taken into account. As a function of (θ_x,θ_y) the spectral radius ρ is continuous (see Fig. 2, for example) but will typically have finite jumps in its first derivative due to a switching from one eigenspace to another when tracking the maximum eigenvalue. In the discrete problem, the sharp localization of unstable wave numbers (as evident from Fig. 2) provides a significant source of mesh dependence. In this work we adhere to the discrete formulation of the problem in order to investigate such dependence as well as to facilitate the detailed comparison between theory and simulation. Of course, increasing the mesh size can be interpreted as evaluating more points on the ρ surface. Therefore, all else constant, uniform flow on a superset of a particular mesh cannot be more stable than on the original mesh. Also apparent from Fig. 2 is that near criticality in parameter space the most unstable wave number can have both x and y dependence. In contrast, Sterling and Chen [1] reported results based on the assumption that the most unstable modes were 1D with $k_y=0$. Indeed, Fig. 2 corresponds to an unstable regime that would appear stable under such a supposition.

In hydrodynamics, large-Reynolds-number $(R=LU/\nu)$ flows are of considerable importance and provide the motivation for attempting to let $\tau\rightarrow 1/2$ in LB simulations. Zero viscosity is a singular limit of the Navier-Stokes equations, but appears to be a regular limit within the LB stability theory, in that the ρ surface of Fig. 2 only gradually deforms as τ is perturbed from 1/2 (see Fig. 2 as a graphical indication of this). It then seems reasonable to study stability *at* $\tau=1/2$ [1] with the understanding that a ''small'' increase from this value would result in a ''small'' change in the reported stability curves.

For model LB7, Figs. 3 and 4 display stability boundaries at $\tau=1/2$ as a function of the model parameter α together with the results of actual simulations in a doubly periodic domain. The simulations were initialized with constant density and the desired uniform mean velocity using the associated equilibrium distribution function F_d. Instabilities are dramatic and easily detected by monitoring, for example, $\max_{\mathbf{x},d} f_d(\mathbf{x},t)$ during the course of the simulation and announcing ''instability'' when and if it exceeds a predefined value like 1 or 10^6. Such criteria are rather arbitrary, but the practical difference between any reasonable criterion aimed at detecting instability seems to be only a matter of a few time steps.

The agreement between theory and simulation is evident in Figs. 3 and 4. It is interesting that the theory predicts a *dramatic* reduction in stability should the mass distribution parameter α be lowered below a slightly mesh-dependent value. Based on these findings, it seems advantageous to have, at equilibrium, roughly 1/2 or more of the mass distributed in the rest particle state when using LB7. A similar sequence of plots for model LB9 is presented in Fig. 5. There, the stable region for even the smallest amplitude uniform flow shrinks to a tiny island in (α,β) parameter space. The values (4/9,1/9) suggested by Qian *et al.* [5] based on maintaining Galilean invariance and isotropy of the fourth-order velocity tensor continue to remain on the stable side as the mesh is refined. For this reason and simplicity, their parameter values are adopted when investigating the influence of other variables like mesh size and τ on stability. Notable (see Fig. 6) is the trendy increase in stability with τ. Simulations are again performed to verify aspects of these findings and four plots intended to relay a feeling for the growth rate of the instabilities are given. If the mesh size is doubled [15], then the stability curve can only move to the left, yielding a larger unstable regime. In Fig. 7 the neutral stability curves for mesh sizes ranging from 2^3 to 2^9 are presented. As the mesh size increases the stability curves tend to converge but retain greatest disparity near $\tau=1/2$. Unfortunately, it is not clear from these limited results whether the curves above approach the origin of the plot, indicating instability of any uniform flow as the mesh size increases to infinity. It is interesting that the 2D ''turbulent'' simulations of Martinez *et al.*. [8] with $N_x=N_y=512$ (denoted by ''○'' in Fig. 7) lie so close to the corresponding linear stability boundary for uniform flow (the farthest curve to the left in the same figure).

IV. INSTABILITY ASSOCIATED WITH BACKGROUND SHEAR

In the previous section it was demonstrated that numerical instabilities could be encountered when using BGK-type lattice Boltzmann methods to simulate uniform flow, itself an exact and physically stable solution of the Navier-Stokes equations in the periodic domain. The more general utility of the instability criteria developed therein lies in the belief that even complicated flows have regions of approximate uniformity.

Thematically similar reasoning prompted the investigation of the simple class of periodic shear layers:

$$\mathbf{u}=U(t)\cos\left(k\frac{2\pi}{L_y}y\right)\hat{\mathbf{i}}. \tag{25}$$

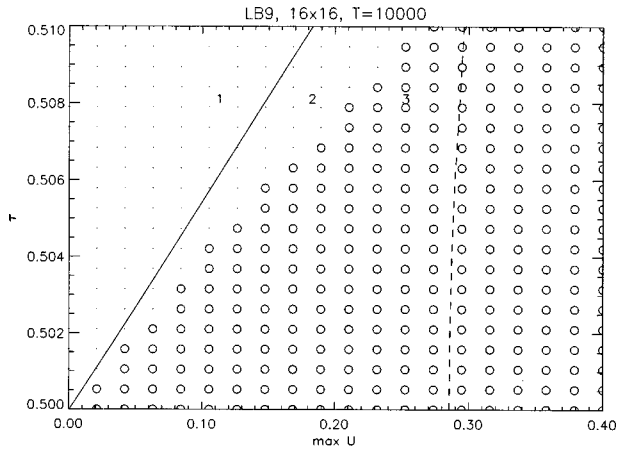

FIG. 9. LB9 neutral stability curve (solid curve) and results of simulations for $k=1$ shear profiles on a 16×16 mesh. The regions denoted by a ''○'' are clearly unstable by $T=10\,000$ and increasing T does not substantially change this plot. Also plotted (dashed curve) for reference is the uniform flow stability boundary for this mesh size.

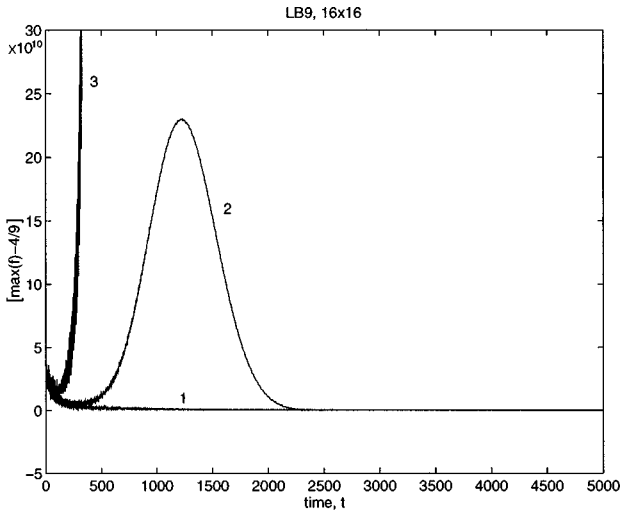

FIG. 10. A measure of instability is plotted for simulations in the regions marked with 1, 2, and 3 in Fig. 9. Both theory and simulation agree that 1 and 3 are, respectively, stable and unstable. The theory's claim that 2 is unstable is based on its clear initial instability. The subsequent restabilization of 2 occurs later in time apparently due to the decay of the basic shear from the unstable to the stable region of parameter space—all before the instability has matured beyond control.

Exact solutions having this form exist for both the NS and LB9 equations though with slightly differing expressions for $U(t)$. (See Appendix B for further comparisons along these lines.)

Extrapolating from the theory of inviscid fluids one would expect initial flows of higher wave number k to be unstable to flows of lower wave number [16], at least in the limit of small viscosity. Figure 8 demonstrates this instability by plotting maximal horizontal and vertical velocities during a LB9 simulation initialized with a $k=2$ mean shear wave along with smaller amplitude noise. Instabilities leading to a $k=1$ mode are evident from the change in the rate of dissipation (slope on this plot) well above the noise level. It is a curiosity that the flow ends up essentially orthogonal to its initial direction. The existence of these inviscid instabilities for $k>1$ suggests that $k=1$ is unique among this class as a quiescent place in which spurious numerical instabilities can be easily identified and studied. This limitation is apparently the price paid for retaining periodicity in y. Even so, significant stability restrictions beyond those based on uniform flow can be obtained by investigating the single shear mode $k=1$, and the results of such investigations are now reported.

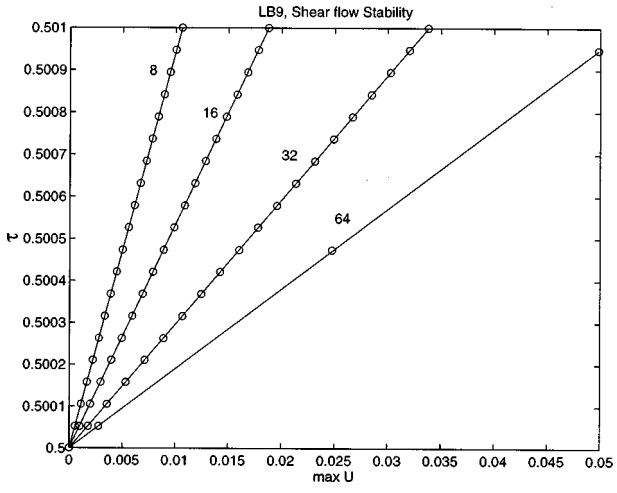

FIG. 11. LB9 shear stability boundaries (near $\tau=1/2$) for mesh sizes 8, 16, 32, and 64. The linearity of each curve provides a maximal Reynolds number criterion if the mesh size is considered fixed.

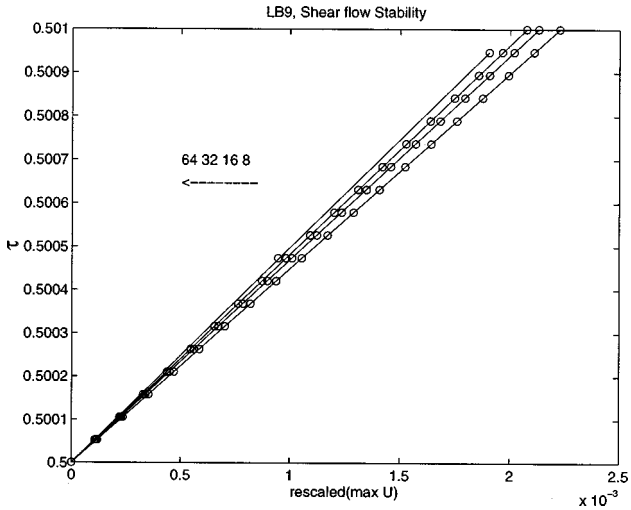

FIG. 12. The data of Fig. 11 under the transformation $U\rightarrow U/N^{0.8}$. If the data under this scaling continue to move to the left as the mesh size is increased, then an *instability* criterion based on $U/N^{\alpha}>(\text{const})(\tau-1/2)$ (where the constant is determined by the rightmost curve) can be derived.

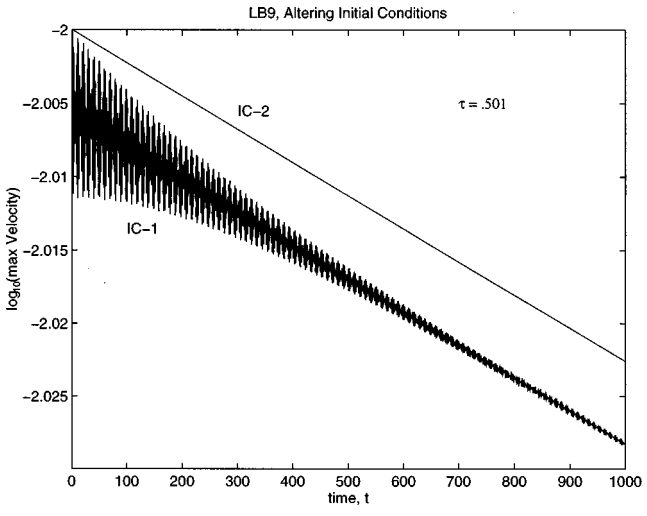

FIG. 13. The results of two simulations at $\tau=0.501$ having *identical* macroscopic but *different* microscopic initial conditions. The usual local equilibrium distribution was used to initialize the run denoted by the lower curve (IC-1). Note the $O(1/(\tau-\frac{1}{2}))$ time scale for relative decay of the highly oscillatory non-NS modes. The upper curve (IC-2) corresponds to a run initialized with a projected form of the equilibrium distribution.

To check the theory, the stability boundary for $k=1$ on 16×16 mesh is calculated and displayed together with the results of actual simulations in Fig. 9. The agreement between theory and simulation seems not as impressive as for the case of uniform flow. Note, however, that agreement is better at smaller values of τ, consistent with the explanation that the discrepancy is merely due to the decay of the basic shear which is not accounted for in the theory laid forth here. Indeed, further evidence of the reasonability of this interpretation is given in Fig. 10 wherein the time evolution of the flow is monitored in various stable and unstable regions of parameter space. One could reasonably construct a quasi-steady version of the theory to account for the decaying amplitude of the basic shear, but we shall resist as our primary interest lies in investigating stability as $\tau\rightarrow1/2$ (the limit of small viscosity), a region wherein this effect is minimized. In this region, results for several different mesh sizes are presented in Fig. 11. First note that all of the curves go through the $(U_{\max},\tau-1/2)$ origin showing that, in contrast to the results based on uniform flow, stability requires that the amplitude of the background field approach zero as $\tau\rightarrow1/2$. Second, each curve is near linear, providing a maximal Reynolds number or $\nu<c_0u$ type criterion for fixed mesh size. This is a much larger region of instability than that conjectured by Rothman and Zaleski [17], i.e., $\nu<c_0u^2$, based on the 1D model of Qian *et al.* [18]. It also follows that, of the three methods to increase the flow's Reynolds number (i.e., increasing N, decreasing τ, and increasing u), only increasing the mesh size retains the possibility of numerical stability. The *instability* criterion $N<R^{0.56}$ is obtained from these data by supposing a continued leftward trend, as displayed in Fig. 12, of the data with increasing mesh size. This criterion constrains N close to the accuracy requirements based on the extent of the Kolmogorov-Batchelor-Kraichnan inertial range in 2D isotropic turbulence, i.e., $N\approx R^{1/2}$.

The type of stability analysis undertaken by Sterling and Chen [1] and refined and extended in this paper seems accurate and effective in delineating clearly unstable regions of parameter space [19] associated with the lattice Boltzmann simulation of fluid flows. Nonperiodic boundary conditions could potentially modify stability by altering the effective local Reynolds number of the mean flow and, perhaps more dangerously, by sufficiently perturbing the spectral problem. Such boundary conditions would also permit other classes of physically stable flows to be investigated for purely numerical instabilities and thereby provide possible refinements on the regions of instability described here.

ACKNOWLEDGMENTS

We are grateful to Dr. Alireza Setayesh and Dr. Xiaowen Shan for helpful discussions relating to this work. This work was supported by the USAF, Phillips Laboratory, Geophysics Directorate, under Contract No. F19628-93-C-0023.

APPENDIX A

Details of models LB7 and LB9 follow.

1. Hexagon-7 (2D)

BGK collision operator: $\mathbf{\Omega}=-\frac{1}{\tau}\,\mathbf{I}$

velocity vectors: $\mathbf{e}_d=\mathbf{0}, \quad d=0$

$\mathbf{e}_d=[\cos(\theta_d),\ \sin(\theta_d)], \quad \theta_d=\pi(d-1)/3, \quad d=1\ldots6$

local mass: $n=\sum_d f_d$

local momentum: $n\mathbf{u}=\sum_d f_d\mathbf{e}_d$

equilibrium: $F_d=n(A_d+B_d\mathbf{e}_d\cdot\mathbf{u}+C_d(\mathbf{e}_d\cdot\mathbf{u})^2+D_d\mathbf{u}\cdot\mathbf{u})$

Jacobian: $\frac{\partial F_d}{\partial f_s}=A_d+B_d\mathbf{e}_d\cdot\mathbf{e}_s+C_d[2(\mathbf{e}_d\cdot\mathbf{e}_s)(\mathbf{e}_d\cdot\mathbf{u})-(\mathbf{e}_d\cdot\mathbf{u})^2]+D_d[2\mathbf{e}_s\cdot\mathbf{u}-\mathbf{u}\cdot\mathbf{u}]$

coefficients: $A_d=\alpha, \quad B_d=0, \quad C_d=0, \quad D_d=-1; \quad d=0$

$A_d=\frac{1-\alpha}{6}, \quad B_d=\frac{1}{3}, \quad C_d=\frac{2}{3}, \quad D_d=-\frac{1}{6}; \quad d=1\ldots6$

parameters: $\tau, \quad \alpha$

viscosity: $\nu=\frac{1}{4}(\tau-\frac{1}{2})$

2. Square-9 (2D)

BGK collision operator: $\mathbf{\Omega}=-\frac{1}{\tau}\mathbf{I}$

velocity vectors: $\mathbf{e}_d=\mathbf{0}, \quad d=0$

$\mathbf{e}_d=[\cos(\theta_d),\ \sin(\theta_d)], \quad \theta_d=\pi(d-1)/2, \quad d=1\ldots4$

$\mathbf{e}_d=\sqrt{2}[\cos(\theta_d),\ \sin(\theta_d)], \quad \theta_d=\frac{\pi(d-5+1/2)}{2}, \quad d=5\ldots8$

local mass: $n=\sum_d f_d$

local momentum: $n\mathbf{u}=\sum_d f_d\mathbf{e}_d$

equilibrium: $F_d=n(A_d+B_d\mathbf{e}_d\cdot\mathbf{u}+C_d(\mathbf{e}_d\cdot\mathbf{u})^2+D_d\mathbf{u}\cdot\mathbf{u})$

Jacobian: $\frac{\partial F_d}{\partial f_s}=A_d+B_d\mathbf{e}_d\cdot\mathbf{e}_s+C_d[2(\mathbf{e}_d\cdot\mathbf{e}_s)(\mathbf{e}_d\cdot\mathbf{u})-(\mathbf{e}_d\cdot\mathbf{u})^2]+D_d[2\mathbf{e}_s\cdot\mathbf{u}-\mathbf{u}\cdot\mathbf{u}]$

coefficients: $A_d=\alpha, \quad B_d=0, \quad C_d=0, \quad D_d=-\frac{2}{3}; \quad d=0$

$A_d=\beta, \quad B_d=\frac{1}{3}, \quad C_d=\frac{1}{2}, \quad D_d=-\frac{1}{6}; \quad d=1\ldots4$

$A_d=\frac{1-4\beta-\alpha}{4}, \quad B_d=\frac{1}{12}, \quad C_d=\frac{1}{8}, \quad D_d=-\frac{1}{24}; \quad d=5\ldots8$

parameters: $\tau, \quad \alpha, \quad \beta$

viscosity: $\nu=\frac{1}{3}(\tau-\frac{1}{2})$

APPENDIX B

In this appendix it is demonstrated that decaying, perfectly sinuous, shear modes exist in the periodic domain for the LB9 equations. Comparison with solutions of the Navier-Stokes equations indicates that $\tau=1$ provides optimal accuracy in time.

Periodic solutions of

$$f_d(\mathbf{x}+\mathbf{e}_d,t+1)=f_d(\mathbf{x},t)-\frac{1}{\tau}\{f_d(\mathbf{x},t)-F_d(n(\mathbf{x},t),\mathbf{m}(\mathbf{x},t))\} \tag{B1}$$

(where $F_d=n[A_d+B_d\mathbf{e}_d\cdot\mathbf{u}+C_d(\mathbf{e}_d\cdot\mathbf{u})^2+D_d\mathbf{u}\cdot\mathbf{u}]$ has appropriate coefficients for LB9) are sought which maintain the macroscopic properties

$$n(\mathbf{x},t)\equiv\sum f_d=n_0,$$

$$\mathbf{m}(\mathbf{x},t)=n\mathbf{u}\equiv\sum f_d\mathbf{e}_d=[u^te^{iky}+\text{c.c.}]\hat{\mathbf{i}}. \tag{B2}$$

The mesh size need not be specified as it is absorbed into the resolution wave number k, and the time dependence can be elevated to a superscript on the remaining variables due to the LB discretization, i.e., $t=0,1,2,\ldots$. Inserting the postulated form

$$f_d(\mathbf{x}+\mathbf{e}_d,t)=a_d^t+[b_d^te^{iky}+c_d^te^{2iky}+\text{c.c.}] \tag{B3}$$

into Eq. (B1) and requiring closure and consistency results in the dynamical equations

$$a_d^{t+1}=(1-\tau^{-1})a_d^t+\frac{n_0}{\tau}[A_d+2(C_d(\hat{\mathbf{i}}\cdot\mathbf{e}_d)^2+D_d)|u^t|^2], \tag{B4}$$

$$e^{ik(\hat{\mathbf{j}}\cdot\mathbf{e}_d)}b_d^{t+1}=(1-\tau^{-1})b_d^t+\frac{n_0}{\tau}[B_d(\hat{\mathbf{i}}\cdot\mathbf{e}_d)u^t], \tag{B5}$$

$$e^{2ik(\hat{\mathbf{j}}\cdot\mathbf{e}_d)}c_d^{t+1}=(1-\tau^{-1})c_d^t+\frac{n_0}{\tau}[C_d(\hat{\mathbf{i}}\cdot\mathbf{e}_d)^2+D_d](u^t)^2, \tag{B6}$$

and constraints

$$\sum a_d^t=n_0, \quad \sum b_d^t=0, \quad \sum c_d^t=0,$$

$$\sum(\hat{\mathbf{i}}\cdot\mathbf{e}_d)a_d^t=0, \quad \sum(\hat{\mathbf{i}}\cdot\mathbf{e}_d)b_d^t=n_0u^t, \quad \sum(\hat{\mathbf{i}}\cdot\mathbf{e}_d)c_d^t=0, \tag{B7}$$

$$\sum(\hat{\mathbf{j}}\cdot\mathbf{e}_d)a_d^t=0, \quad \sum(\hat{\mathbf{j}}\cdot\mathbf{e}_d)b_d^t=0, \quad \sum(\hat{\mathbf{j}}\cdot\mathbf{e}_d)c_d^t=0.$$

The question of existence becomes: For fixed k, n_0, and u^0, can initial values for the complex sequences b_d^t, c_d^t and real sequences a_d^t be chosen so that the stated dynamics maintain the above constraints. To see that the answer is yes, consider, for example, only the ''a'' equations. If at any time t the following is true,

$$a_1^t=a_3^t,\quad a_2^t=a_4^t,\quad a_5^t=a_6^t=a_7^t=a_8^t,\quad \text{and } \sum a_d^t=n_0, \tag{B8}$$

then two things can be said; first the ''a'' constraints of Eq. (B7) are clearly satisfied and secondly the relations (B8) will continue to hold at all later times. The last statement follows by considering various combinations of the dynamical equations, like $(a_1-a_3)^{t+1}=(1-\tau^{-1})(a_1-a_3)^t$. It is helpful to note $\Sigma A_d=1$ and $\Sigma C_d(\hat{\mathbf{i}}\cdot\mathbf{e}_d)^2+D_d=0$ to verify $\Sigma a_d^{t+1}=\Sigma a_d^t=n_0$. Similar considerations for the ''b'' and ''c'' equations suggest initially assigning values so:

$$a_1^0=a_3^0,\quad a_2^0=a_4^0,\quad a_5^0=a_6^0=a_7^0=a_8^0,\quad \sum a_d^0=n_0, \tag{B9}$$

$$b_0^0=0,\quad b_1^0=-b_3^0,\quad b_2^0=-b_4^0,\quad b_5^0=-b_6^0,$$
$$b_7^0=-b_8^0,\quad \sum(\hat{\mathbf{i}}\cdot\mathbf{e}_d)b_d^0=u^0, \tag{B10}$$

$$c_1^0=c_3^0,\quad c_2^0=c_4^0,\quad c_5^0=c_6^0=c_7^0=c_8^0,\quad \sum c_d^0=0. \tag{B11}$$

A concrete example of such an initial condition (one satisfying the class described above) derives from the equilibrium distribution F_d,

$$a_d^0=n_0\{A_d+2[C_d(\hat{\mathbf{i}}\cdot\mathbf{e}_d)^2+D_d]|u^0|^2\}, \tag{B12}$$

$$b_d^0=n_0B_d(\hat{\mathbf{i}}\cdot\mathbf{e}_d)u^0, \tag{B13}$$

$$c_d^0=n_0[C_d(\hat{\mathbf{i}}\cdot\mathbf{e}_d)^2+D_d](u^0)^2. \tag{B14}$$

Therefore solutions of the discrete LB9 equations having the exact form (B2) exist.

To describe the macroscopic time dependence u^t further analysis of the central and self-closing ''b'' equation (B5) is required. The particularly simple and solely macroscopic equation

$$u^{t+1}=\frac{2+\cos(k)}{3}u^t\quad(\tau=1) \tag{B15}$$

is obtained by setting $\tau=1$ and taking appropriate sums of Eq. (B5). Comparing this with the corresponding Navier-Stokes equation [20]

$$u^{t+1}=e^{-k^2/6}u^t \tag{B16}$$

gives a remarkably small difference $\sim k^6/3240$ (for small k) in decay rates. Unfortunately, we shall find $\tau=1$ unique in these regards in that other non-NS type behavior is to be expected from LB9 at other values of τ, especially in the important limit $\tau\to 1/2$.

For general τ, the dynamics of u^t can be written as $n_0u^t=[1\ 1\ 1]\cdot\mathbf{b}^t$ where

$$\mathbf{b}^{t+1}=\mathcal{A}\mathbf{b}^t,$$

$$\mathcal{A}\equiv\begin{bmatrix} 1-\frac{1}{3\tau} & \frac{2}{3\tau} & \frac{2}{3\tau} \\ e^{-ik}\frac{1}{6\tau} & e^{-ik}\left(1-\frac{5}{6\tau}\right) & e^{-ik}\frac{1}{6\tau} \\ e^{ik}\frac{1}{6\tau} & e^{ik}\frac{1}{6\tau} & e^{ik}\left(1-\frac{5}{6\tau}\right) \end{bmatrix},$$

and

$$\mathbf{b}^t\equiv\begin{bmatrix} b_1^t-b_3^t \\ b_5^t-b_6^t \\ b_8^t-b_7^t \end{bmatrix}.$$

Though an exact eigenanalysis and therefore closed form solution of the above iteration equation exists, approximate expressions for the eigenvalues in the limit of small k with emphasis on the case where $\tau\leqslant 1$ seem more digestible for our purposes, i.e.,

$$\lambda_1\sim 1-\nu k^2+\left\{\frac{1}{2}\nu^2+\left(3\nu^3-\frac{1}{12}\nu\right)\right\}k^4-\cdots, \tag{B17}$$

$$\lambda_{2,3}\sim\left(1-\frac{1}{\tau}\right)\left[1\pm i\sqrt{\frac{2}{3}}k-\cdots\right], \tag{B18}$$

where we have set $\nu=(\tau-1/2)/3$ in the expression for λ_1 to facilitate comparison with the corresponding NS eigenvalue

$$\lambda_{\mathrm{NS}}\sim 1-\nu k^2+\tfrac{1}{2}\nu^2k^4-\cdots.$$

Setting $\tau=1$ simultaneously removes the non-NS modes and decreases the error of the physical mode from $O(k^4)$ to $O(k^6)$. However, near $\tau=1/2$, the ratio of eigenvalues reveals that one must wait at least $O((\tau-\frac{1}{2})^{-1})$ in time before the nonphysical modes are relatively decayed (see Fig. 13). For the simple sinuous profiles discussed here, this unfortunate time scale can be easily avoided by altering the microscopic initial conditions slightly from those based on the equilibrium distribution. Indeed the results (Fig. 13) of a run beginning with a *projected* form of the equilibrium distribution (onto the λ_1 eigenspace) show no such unphysical oscillations. It is not clear whether this idea could be reasonably extended to improve general LB9 simulations of low viscosity fluids.

[1] J.D. Sterling and S. Chen, J. Comput. Phys. **123**, 196 (1996).
[2] G. McNamara and G. Zanetti, Phys. Rev. Lett. **61**, 2332 (1988).
[3] F.J. Higuera, S. Succi, and R. Benzi, Europhys. Lett. **9**, 345 (1989).
[4] J.M.V.A. Koelman, Europhys. Lett. **15**, 603 (1991).
[5] Y.H. Qian, D. D'Humieres, and P. Lallemand, Europhys. Lett. **17**, 479 (1992).
[6] U. Frisch, B. Hasslacher, and Y. Pomeau, Phys. Rev. Lett. **56**, 2505 (1986).
[7] It would be correct to say that the scale at which the desired partial differential equation is approached is vastly different for the two methods, but no formal theory addressing this disparity has been put forth in the literature.
[8] D.O. Martinez, W.H. Matthaeus, S. Chen, and D.C. Montgomery, Phys. Fluids **6**, 1285 (1994).
[9] F.J. Higuera and J. Jimenez, Europhys. Lett. **9**, 663 (1989).
[10] P. Bhatnagar, E.P. Gross, and M.K. Krook, Phys. Rev. **94**, 51 (1954).
[11] This is a general representation for fully complex $f_d(x,y,t)$. One may want to restrict the stability analysis to allow for only real $f_d(x,y,t)$. This issue may be particularly important at the highest frequencies, $-N_x/2$ and $-N_y/2$. However, ignore this point for the moment.
[12] By ''highest'' we mean those not representable on the given lattice. In general these frequencies will be aliased back upon those that are representable; however, this projection is assumed small and neglected in this work.
[13] But computationally other instabilities that vary in space and time may occur and are considered later in this section.
[14] Note that if one is treating a hexagonal mesh by subsuming it within a larger rectangular mesh (as we have done here), then this will put additional restrictions on the allowable wave numbers.
[15] Doubled, since we wanted to preserve the superset argument.
[16] P.G. Drazin and L.N. Howard, in *Advances in Applied Mechanics*, edited by G. Kuerti (Academic Press, New York, 1966), Vol. 7.
[17] D.H. Rothman and S. Zaleski, Rev. Mod. Phys. **66**, 1417 (1996).
[18] Y.H. Qian, D. D'Humieres, and P. Lallemand, in *Advances in Kinetic Theory and Continuum Mechanics*, edited by R. Gatignol and Soubbaramayer (Springer, Berlin, 1991).
[19] A potentially large space including free model parameters, mesh type and size, indicators of background flow amplitude and gradients, etc..
[20] The value of the viscosity at $\tau=1$ is taken from the accepted LB9 conversion $\nu=(\tau-1/2)/3$.